One Earth

Article

Geospatial analysis of regional climate impacts to accelerate cost-efficient direct air capture deployment

Graphical abstract

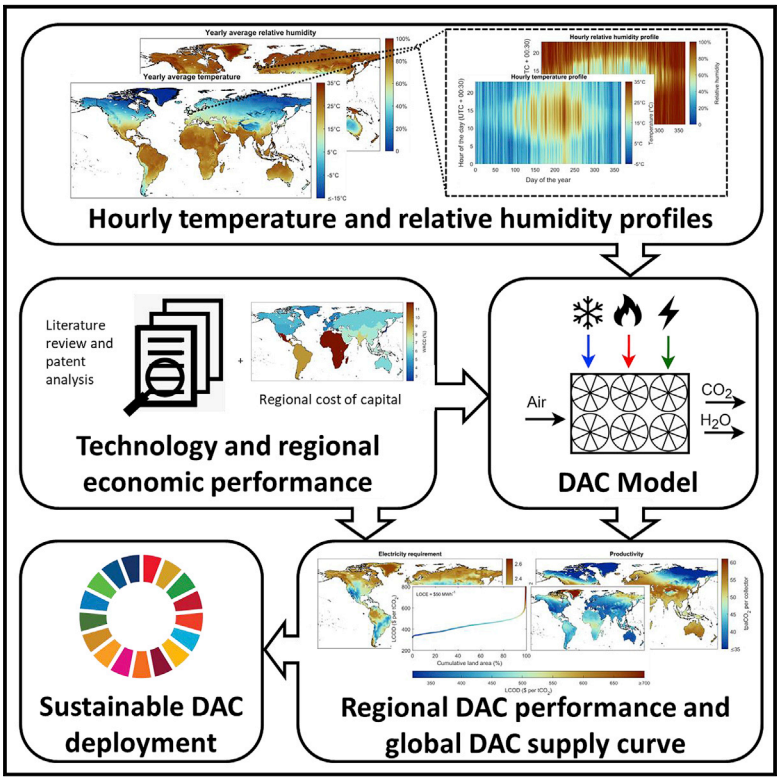

Highlights

- Regional DAC performance is impacted by daily and seasonal weather variation
- Least-cost DAC sites are identified based on regional climate and cost of capital
- DAC using amine-functionalized sorbent performs better in cold and dry regions
- Assuming $50/MWh electricity cost, levelized cost of DAC is $320–$540/tCO_2

Authors

Marwan Sendi, Mai Bui, Niall Mac Dowell, Paul Fennell

Correspondence

niall@imperial.ac.uk (N.M.D.), p.fennell@imperial.ac.uk (P.F.)

In brief

Removing CO_2 directly from the air emerges as a viable approach to meeting the Paris climate targets. Since direct air capture (DAC) is climate sensitive, understanding the effect of regional climate on DAC performance is essential for cost-effective deployment, yet knowledge remains limited. Here, we use a systematic model, including hourly weather data between 2016 and 2020 to identify key regions with the best techno-economic performance. Results show that a drier and colder climate is techno-economically favorable, but sub-ambient temperatures (e.g., −15°C) will not be suitable.

Sendi et al., 2022, One Earth *5*, 1153–1164
October 21, 2022
https://doi.org/10.1016/j.oneear.2022.09.003

CellPress

One Earth

CellPress
OPEN ACCESS

Article

Geospatial analysis of regional climate impacts to accelerate cost-efficient direct air capture deployment

Marwan Sendi,[1,2] Mai Bui,[2,3] Niall Mac Dowell,[2,3,*] and Paul Fennell[1,4,*]
[1]Department of Chemical Engineering, Imperial College London, London SW7 2AZ, UK
[2]The Sargent Centre for Process Systems Engineering, Imperial College London, London SW7 2AZ, UK
[3]Center for Environmental Policy, Imperial College London, London SW7 1NE, UK
[4]Lead contact
*Correspondence: niall@imperial.ac.uk (N.M.D.), p.fennell@imperial.ac.uk (P.F.)
https://doi.org/10.1016/j.oneear.2022.09.003

SCIENCE FOR SOCIETY In addition to the rapid decarbonization of modern society, if we are to successfully achieve net-zero emissions targets by 2050, massive amounts of carbon dioxide (CO_2) will need to be directly removed from the atmosphere (i.e., billions of tons per year). Direct air capture (DAC), while expensive, has emerged as a promising CO_2 removal approach relative to other methods due to deployment flexibility and its relatively small land footprint. However, DAC technology is sensitive to temperature and humidity, meaning that DAC performance (and thus capital and operational costs) varies under different climate conditions. Given the expensive nature of the technology, the need to secure public and private investment, and the urgent need to achieve regional net-zero emissions targets, it is crucial that we identify sites where DAC facilities can deliver optimal techno-economic performance. The results presented in this article reveal that one-quarter of the global land surface is likely to be unfavorable for the cost-effective deployment of DAC facilities. Developing DAC technologies that are adapted to regional climate could provide policymakers more certainty around cost.

SUMMARY

Carbon dioxide (CO_2) removal from the atmospheric will be essential if we are to achieve net-zero emissions targets. Direct air capture (DAC) is a CO_2 removal method with the potential for large-scale deployment. However, DAC operational costs, and thus deployment potential, is dependent on performance, which can vary under different climate conditions. Here, to further develop our understanding of the impact of regional climate variation on DAC performance, we use high-resolution hourly based global weather profiles between 2016 and 2020 and weighted average capital costs to obtain DAC regional performance and levelized cost of DAC (LCOD). We found that relatively cold and drier regions have favorable DAC performance. Moreover, approximately 25% of the world's land is potentially unsuitable due to very cold ambient temperatures for a substantial part of the year. For the remaining regions, the estimated LCOD is \$320–\$540 per tCO_2 at an electricity cost of \$50 MWh^{-1}. Our results improve the understanding of regional DAC performance, which can provide valuable insights for sustainable DAC deployment and effective climate action.

INTRODUCTION

Direct air capture (DAC) combined with carbon dioxide (CO_2) storage (DACS) is one option in a portfolio of negative emission technologies required to remove up to 10 Gt of CO_2 from the atmosphere per year by 2050, reaching a scale of 20 $GtCO_2$ per year by 2100.[1–5] DAC technologies use engineered materials to remove CO_2 directly from the air, before storing the CO_2 permanently by injecting it underground into a suitable rock formation, or mineralization.[6–8] The stored CO_2 can be easily quantified, monitored, and verified, making it easy for firms and governments to trade and invest.[2,9] Although the permanent storage of the captured CO_2 should be prioritized to achieve climate goals, the utilization of CO_2 captured via DAC can have different applications and commercial opportunities, such as sustainable fuel production and microalgae cultivation.[10] Moreover, the modularity of DAC units makes their deployment scalable and offers more geographic flexibility for deployment.[2,5,9] The

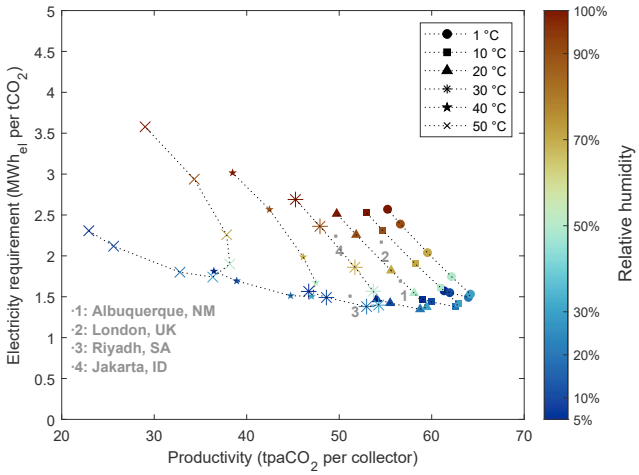

Figure 1. Performance of SA-VTSA at different ambient temperatures and relative humidity

The electricity requirement includes both energy consumed by the heat pumps (providing process heat and steam), fans, vacuum pumps, and compressors. The different symbols correspond to different ambient temperatures, and the color corresponds to different relative humidity, where the labeled tick marks on the relative humidity axis correspond to the humidity of the different sampled points. The four gray markers show the average yearly productivity and its average electricity consumption from Figure 3 for the four locations: (1) Albuquerque, New Mexico; (2) London, UK; (3) Riyadh, Saudi Arabia; and (4) Jakarta, Indonesia. These locations represent cold dry, cold humid, hot dry, and hot humid climates, respectively. The hourly performance profiles for the four locations are shown in Figures S1–S4.

combination of these features makes DAC potentially very attractive as a CO_2 removal technology.

The most developed DAC technologies employ either absorption or adsorption.[1,2,11,12] Absorption-based DAC processes typically utilize an aqueous alkali hydroxide solution, such as potassium hydroxide (KOH), and require high temperatures of about 900°C for sorbent regeneration (i.e., calcination); and, depending on the ambient conditions, water loss can be significant.[13] In contrast, adsorption DAC utilizes amine-functionalized solid sorbents, which are regenerated using relatively low temperatures of around 100°C and co-adsorbs water from the air, generating water as a by-product.[14–16] The lower sorbent regeneration temperature of the solid sorbent process provides a more favorable exergy demand compared with the KOH-based system and more extensive process coupling options to cheaper thermal energy sources, such as geothermal and nuclear power plants.[17–19] Moreover, the solid sorbent process showed that it outperforms the KOH-based system in terms of life-cycle analysis.[20]

Previous assessments of solid sorbent-based DAC have focused on developing and optimizing different cycle configurations or processes.[17,21–25] These assessments only considered one ambient condition when evaluating process performance or economics,[17,21–24] or only investigated adsorption behavior for different weather conditions without providing comprehensive process performance (i.e., productivity and energy requirement) and economics metrics under these conditions.[25] Although one study analyzed the cost of solid sorbent DAC globally, this was based on a fixed DAC performance corresponding to one ambient condition and a fixed weighted average capital cost (WACC).[26] However, the ambient conditions of air vary widely across different regions of the world, with daily and seasonal variations. Consequently, the performance of DAC plants will be highly dependent on the climate and weather fluctuations of their location.[16] This is also the case for WACC as it can represent the cost of rising investment funding which also varies across regions. Understanding the interplay between DAC plant performance and different climate conditions can help identify regions around the world where DAC plants perform optimally. This, in addition to understanding how WACC affects DAC cost in different regions, can lead to cost-effective and sustainable deployment of DAC. In sum, our understanding of the effects of region-specific climate and WACC on DAC performance and cost remains limited.

Here, we comprehensively evaluate the solid sorbent DAC performance globally using high-resolution temporal and spatial weather data. The cycle performance of DAC based on steam-assisted vacuum-pressure temperature swing adsorption (SA-VTSA) technology and best-in-class solid sorbent (i.e., amine-functionalized) is assessed using a dynamic adsorption model at different ambient temperatures and relative humidity (RH).[21,27] The obtained performance data are then used to evaluate how DAC plants perform globally using hourly weather data. This DAC performance information is used along regional WACC to estimate the levelized cost of DAC (LCOD) and generate a global DAC supply curve at different fixed levelized cost of electricity (LCOE). Regional LCOD can provide an average cost of the captured CO_2 by DAC over the DAC plant lifetime. The LCOD accounts for the capital and operating cost of process equipment, as well as the cost of sorbent and electricity (Equation 37); it considers the cost of CO_2 capture and compression to 150 bar, but excludes the CO_2 storage costs. Our findings show how climate and WACC affects regional DAC performance and cost. Owing to regional variations, the LCOD can range between \$320 and \$540 per tCO$_2$ at LCOE of \$50 MWh^{-1}, excluding the regions with low performance (i.e., average ambient temperatures below −15°C for a substantial part of the year). Understanding the effect of regional variations on DAC techno-economic performance is important in the context of achieving sustainable greenhouse gas removal targets and accelerating the transformation to a net-zero emissions future. The global DAC supply curve can be used to map the deployment opportunities for DAC, for instance, sustainable fuel production or sharing large-scale CO_2 transport and storage infrastructure, for example, in low-carbon industrial clusters.

RESULTS AND DISCUSSION

Effect of ambient conditions at a process level

As shown by Figure 1, weather conditions (i.e., ambient temperature and RH) can have a major impact on DAC plant performance. Consequently, assuming constant conditions as done in previous DAC assessments (e.g., 20°C and RH of 50%) would not account for the varying DAC plant performance when conditions change with the seasons and regions. This impact can be seen in terms of productivity and energy requirements, both of which impact the cost of DAC. When comparing the yearly

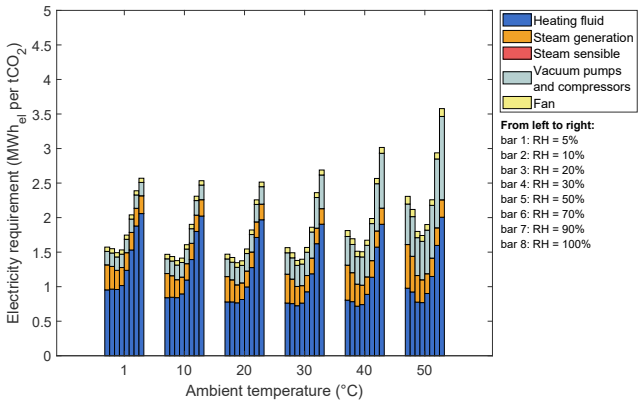

Figure 2. Electricity requirement breakdown

Air source heat pumps are used to provide thermal energy to the heating fluid that is used to heat the sorbent bed in the first part of the desorption step (blue electricity requirement). Steam is then used to purge the sorbent bed where steam electricity requirement is broken into electricity (by the heat pumps) needed to preheat the steam water supply and the electricity needed (by the heat pumps) to generate the steam. The electricity requirement for preheating the steam water supply is zero for all conditions as this heat requirement is met by the recovered heat from compressing the process gasses (see experimental procedures). The vacuum pumps and compressors maintain the vacuum during the desorption process and compress the CO_2 stream to 150 bar. Fans push the air through the CO_2 collector during the adsorption step. Figure S7 shows the energy requirement breakdown in terms of thermal energy demand.

average DAC plant performance of the four sampled locations shown in Figure 1 to a fixed DAC plant performance at a temperature of 20°C and RH of 50%, it can be seen that the yearly average plant productivity would be overestimated for the four locations. Moreover, for three of the four locations (Albuquerque, London, and Jakarta), the yearly average electricity requirement is underestimated. Figures S1–S4 shows hourly performance profiles for the four sample locations considered in Figure 1.

Within the range of temperature (1°C–30°C) and RH (5%–100%) considered, each CO_2 collector can capture between 45.3 and 64.2 tons per annum of CO_2 ($tpaCO_2$) with electricity requirements of 1.35–2.69 MWh_{el} per tCO_2. Within the same temperature and RH range considered, it can be seen from Figure 1 that change in RH has an observable effect on both electricity requirement and productivity. In contrast, temperature change only has a noticeable effect on productivity. For this reason, RH can be considered to have more influence on DAC performance than temperature within this temperature range. However, as temperature increases to 40°C and 50°C, the effect of temperature on electricity requirement becomes more apparent. Figures S5 and S6 show the effect of temperature and RH on productivity and electricity requirement.

An electricity requirement breakdown is shown in Figure 2. In general, depending on the ambient temperature, the collector productivity increases while electricity requirement decreases at mild RH in the range of 20%–60% (Figures 1 and 2). This is mainly because of the enhancement of the CO_2 adsorption on the amine-functionalized sorbent due to the presence of water.[14,16] This enhancement leads to an increase in the CO_2 working capacity, causing improvement in process productivity and energy efficiency. However, this effect is diminished at higher RH as the sorbent water loading increases, leading to an increase in required heat input for sorbent regeneration (Figures 2 and S7), resulting in a longer heating step and decreased productivity (Figure 1). This concurs with lab experiments that involve heating the bed after sorbent saturation with dry CO_2 and wet CO_2 (i.e., moist air).[14] A similar effect happens at high ambient temperatures, where CO_2 working capacity decreases while the sorbent water capacity increases, leading to a higher sorbent regeneration heat input requirement and lower process productivity (Figures 1 and S7). However, this is not apparent in terms of the heat pump's electricity requirement, which provide thermal energy for bed heating and steam generation (Figure 2) due to the higher heat pump coefficient of performance (COP) at higher ambient temperatures.

Moreover, as ambient temperature decreases, the bed heating requirement increases slightly as the sensible heat required to heat the bed to the desorption temperature increases. This is coupled with a lower heat pump COP at lower ambient temperatures, which results in a higher electricity requirement for bed heating as well as steam generation (Figure 2). Finally, as ambient temperature increases, less heat can be removed from the intercoolers between the vacuum pump and compressor stages. This leads to a higher vacuum pump and compressor inlet gas temperature, resulting in higher electricity requirements (Figure 2).

Effect of regional climate on DAC performance and cost

It can be seen from Figure 3 that the CO_2 collector productivity and electricity requirement correlate well with the yearly average temperature and RH, where the productivity has a noticeable correlation with the average temperature and RH, and electricity requirement has only a stronger correlation with the average RH. In general, productivity is higher in low-RH and low-temperature regions. However, the productivity sharply decreases to below 45 $tpaCO_2$ per collector where the temperature drops below −15°C (the minimum assumed operating temperature) for most of the year, e.g., high-latitude regions due to the lower plant capacity factor in these regions. Furthermore, low electricity requirement regions can be found in drier regions with lower average RH.

Here, to analyze regional performance based on climates, regions of the world are aggregated into four groups based on two temperature intervals (cold and hot, with a yearly average temperature below and above 18°C, respectively) and two RH intervals (dry and humid, with yearly RH below and above 65%, respectively). Very cold regions with temperatures below −15°C for more than 30 days per year are excluded due to the low DAC plant productivity. The aggregated four regions—cold dry, cold humid, hot dry, and hot humid—could be found in cold-arid and semi-arid, continental and cooler temperate, hot-arid and semi-arid, and tropical and warmer temperate climates, respectively. Figure 4 shows maps of the four aggregated regions.

Table 1 summarizes the DAC performance metrics with data visualization shown in Figures S8 and S9. When the four regions are compared, the highest DAC plant productivity can be found in cold dry regions where the productivity can reach up to 60.6

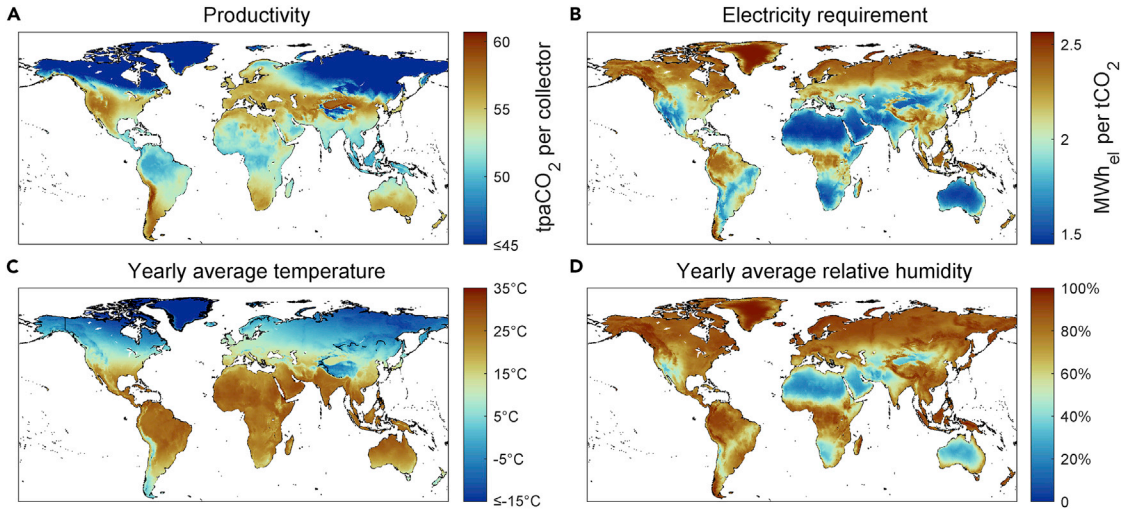

Figure 3. DAC global performance

(A) CO_2 collector productivity obtained using hourly CO_2 production averaged over the year, assuming −15°C as a minimum operating temperature for the DAC plant.

(B) The average electricity requirement for the yearly CO_2 production. The current benchmark DAC solid-sorbent (i.e., Lewatit VP OC 1065)[16] is used when calculating global productivity (A) and electricity requirement (B) where future climate-tailored sorbents can be developed, potentially impacting regional differences in DAC performance. Also, it is assumed that when the temperature is below 1°C, process performance is fixed to the performance of operating at 1°C (see experimental procedures). Global maps for a breakdown of the total electricity requirement (B) into thermal and electric energy requirements can be found in Note S6.

(C) Yearly average temperature.

(D) Yearly average humidity.

$tpaCO_2$ per collector with an average of 56.8 $tpaCO_2$ per collector. This process productivity is coupled with a relatively low electricity requirement with an average of 1.76 MWh_{el} per tCO_2. After that, cold humid regions have better productivity, an average of 54.8 $tpaCO_2$ per collector, compared with hot dry regions, an average of 53.5 $tpaCO_2$ per collector. However, hot dry regions have lower electricity requirements, an average of 1.64 MWh_{el} per tCO_2, compared with cold humid regions, an average of 2.15 MWh_{el} per tCO_2. Finally, hot humid regions have the lowest plant productivity, with an average of 51.6 $tpaCO_2$ per collector, and relatively high electricity requirement, with an average of 2.11 MWh_{el} per tCO_2.

The DAC plant performance in Figure 3 is used to estimate LCOD assuming that the solid sorbent-based CO_2 collectors can be manufactured and purchased at a mid-sized car price of $20,000. This cost estimate was used because similar raw materials[28] and assembly/construction processes that are used to manufacture cars could be used for DAC collectors; the material assessment is shown in Table S1. Moreover, the current solid sorbent-based technology employs modular collectors that are easier to scale out (i.e., adding more collectors to increase the plant capacity) than to scale up (i.e., increasing the collector size to increase the plant capacity). Therefore, as the demand for CO_2 collectors increases, we expect that

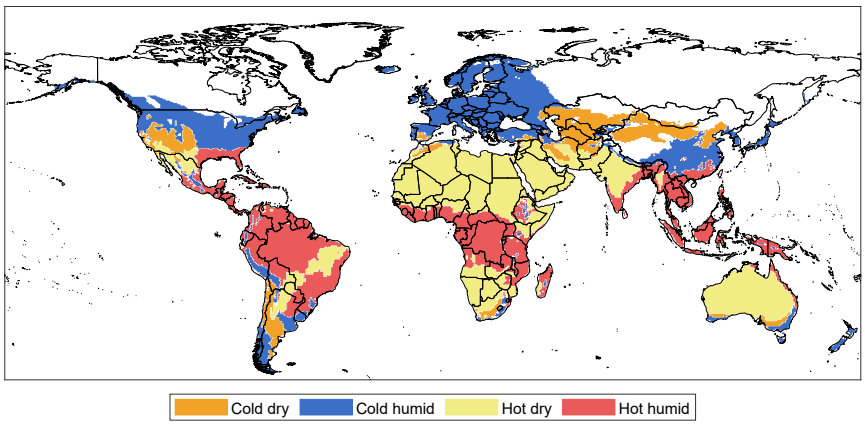

Figure 4. Aggregated climate regions

Aggregation is based on yearly average temperature and relative humidity above and below 18°C and 65%, respectively. Regions where the temperature drops below −15°C more than 30 days per year are excluded.

Table 1. Global DAC performance and LCOD at different climates conditions

Climate conditions	Regions[a]		Productivity per collector ($tpaCO_2$)	Energy requirement (MWh_{el} per tCO_2)	LCOD ($ per tCO_2) LCOE $0 MWh^{-1}	LCOE $50 MWh^{-1}	LCOE $100 MWh^{-1}
Cold (<18°C[b]) dry (RH < 65%)	cold-arid and semi-arid regions in the US, e.g., New Mexico and Wyoming, Southern Spain, and Central Asia	min–max	52.6–60.6	1.50–1.97	240–374	324–469	403–565
		mean	56.8	1.76	277	365	453
Cold (<18°C[b]) humid (RH > 65%)	US states with a continental climate, UK, Europe, East Asia, part of Southern Australia, and New Zealand	min–max	50.4–58.8	1.81–2.56	220–405	320–525	421–645
		mean	54.8	2.15	281	388	496
Hot (>18°C) dry (RH < 65%)	hot-arid and semi-arid regions in the US, e.g., West Texas, Sahara Desert, Middle East, and Australia	min–max	50.0–57.7	1.45–1.94	243–402	327–499	405–596
		mean	53.6	1.64	338	420	501
Hot (>18°C) humid (RH > 65%)	tropical regions in Central and South America, Africa, South India, and Southeast Asia	min–max	48.5–55.8	1.79–2.47	243–421	337–540	432–659
		mean	51.6	2.11	357	462	568

Visualization of the data is shown in Figures S8 and S9.
[a]Figure 4 shows the maps of the different aggregated climate regions.
[b]Regions with more than 30 days of temperatures below −15°C per year are excluded.

these collectors will be mass-produced utilizing automated manufacturing and, more broadly, employing existing automotive industry experience, thus making their cost closer to cars.

The LCOD calculated globally at different LCOE is shown in Figure 5 in terms of supply curves and global maps. The estimated LCOD for the global land at LCOEs of $50 MWh^{-1} and $100 MWh^{-1} is in the range of $320–$1,518 and $403–$1,646 per tCO_2, respectively. These ranges reduce to $320–$540 and $403–$659 per tCO_2 when cold regions with temperatures below −15°C more than 30 days per year are excluded. The remaining regions represent 76% of the global land area. These LCOD are comparable with the cost range suggested in the literature of $100–$600 per tCO_2.[2,29]

LCOD ranges result from different regional WACC (Figure 8) and DAC plant performances, including process productivity and electricity requirements (Figures 3 and 5). Figure S10 shows DAC supply curves when WACC is fixed to 5%, which helps distinguish the effect of regional climate from the effect of WACC variation on LCOD. Lower regional WACCs generally correspond to the lower LCOD range of each climate group shown in Table 1. On average, when a fixed LCOE is assumed, cold dry regions have the cheapest LCOD because of the relatively high process productivity and low electricity requirement. The lower range LCOD for this climate group can be found in some US states with cold dry climate, such as New Mexico and Wyoming, and colder regions in Southern Spain, Southern Australia, and Northwest China. In some cases, cold humid regions can achieve cheaper LCOD than cold dry regions at lower LCOE because they include lower WACC regions, such as Japan, Western Europe, and the UK. However, this is not the case at high LCOE since cold humid regions in general have higher electricity requirements than cold dry regions.

The overall picture is similar when cold humid regions, with better process productivity, are compared with hot dry regions with lower electricity requirements, where cold humid regions can achieve cheaper LCOD at low LCOE, whereas hot dry regions can achieve cheaper LCOD at higher LCOE. This, however, is not reflected in the average LCOD for the two regional climates in Table 1 because cold humid regions include lower WACC regions, such as Japan and Western Europe, and hot dry regions include a large part of Africa where WACC is relatively high. Nonetheless, this can be illustrated from Figure 5 by comparing hot humid regions with moderate WACC, such as Australia and the Middle East, with cold humid regions, such as Europe and the Northern US. At low LCOE (Figure 5A), Europe and the Northern US have cheaper LCOD from the four mentioned regions; then as LCOE increases and reaches $50 MWh^{-1} (Figure 5B), the four regions have comparable LCOD; and as LCOE increases further and reaches $100 MWh^{-1} (Figure 5C), LCOD in Australia and the Middle East starts to become relatively cheaper. Finally, hot and humid regions have the highest average LCOD due to a combination of the low process performance, and the fact that a large portion of these regions consists of Africa and Latin America, where WACC is high.

To put the DAC land requirement into perspective, the land area requirement can be estimated based on the Climeworks plant at Hinwil, where 18 DAC collectors with average productivity of 50 $tpaCO_2$ per collector and a similar size to the one modeled here occupy a land area of 90 m^2 (see Viebahn et al.[31]). Based on this land area requirement and the collector productivity in Table 1, capturing 10 $GtCO_2$ per year using DAC will require 825 km^2 for the maximum productivity of 60.6 $tpaCO_2$ per collector, whereas the minimum productivity of 48.5 $tpaCO_2$ per collector requires 1,031 km^2. This land area range

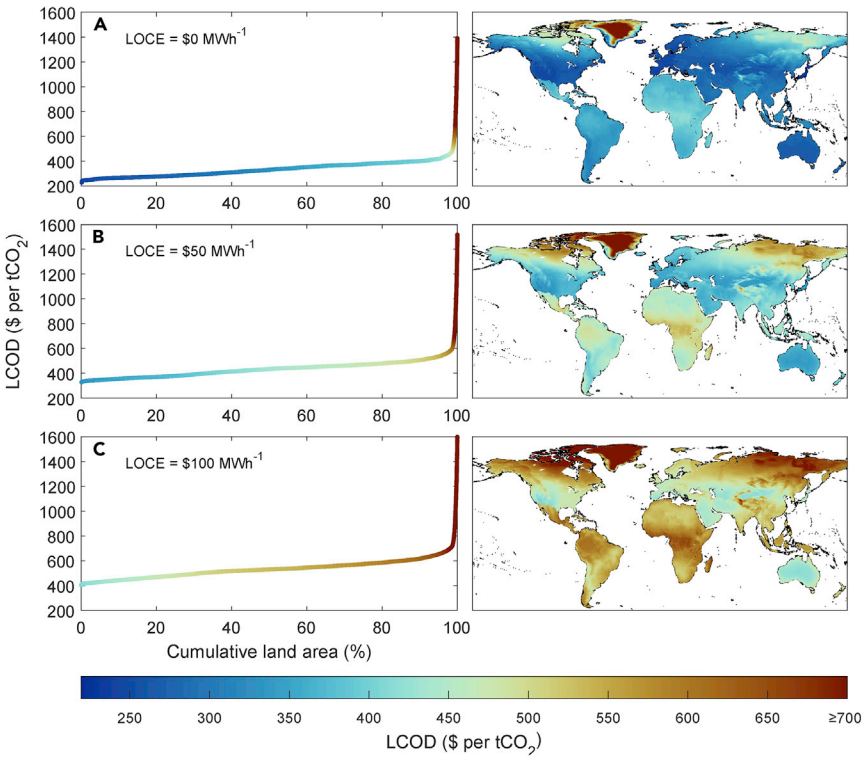

Figure 5. Global cost and supply curve for SA-VTSA

The left figures show the global DAC supply curves at different LCOEs as a function of total land that can deliver DAC at the corresponding levelized cost of DAC (LCOD). The color of the data points of the supply curves matches their location on the corresponding map on the right. Darker blue indicates a cheaper LCOD, and darker brown indicates a more expensive LCOD. The LCOD was calculated using regional WACC,[30] which is shown in Figure 8 (see experimental procedures). For comparison, similar figures are produced at a fixed WACC of 5% and shown in Figure S10.

corresponds to less than 0.001% of the global land area. This amount of DAC can be provided at the cheapest DAC supply cost of \$320 per tCO_2 at an LCOE of \$50 MWh^{-1}. However, this implies that all DAC plants will be constructed in a small area, which might not be practical in terms of actual land availability, energy supply, or the availability of secure CO_2 storage sites. For example, the electricity requirement needed to capture 10 $GtCO_2$ per year is around 14,500–25,600 TWh_{el} per year (Table 1). Supplying this energy by nuclear power will require an additional land area of 3,500–6,200 km^2 based on a land area requirement of 2 km^2 for a 1 GW_{el} nuclear power plant[32] and a capacity factor of 95% (based on nuclear requiring 0.24 m^2/MWh per year). If solar PV is used, the land requirement is 200,000–350,000 km^2, which is based on a land requirement of 13.8 m^2 to produce 1 MWh of solar PV electricity per year.[33] This land requirement for solar PV DAC is 60 times the area requirement of using nuclear power, which is equivalent to 40%–70% the land area of Spain. Here, it should be noted that the land type for different energy sources has different land footprints. For instance, while nuclear power facilities require special licensed land and access to water supply, solar PV is more flexible in its installation, where it can be installed on remote arid lands.

In a more practical approach, sustainable DAC deployment will depend on cheap LCOD based on the regional climate and WACC, the availability of cheap and low-carbon energy sources and access to secure CO_2 storage sites.[34,35] This is in addition to the availability of suitable land for DAC plant deployment and its energy supply, which may be constrained, for instance, due to competition for agricultural land, urbanization, national parks, or having other geological and geographic restrictions (e.g., mountains, forests, bodies of water).

Conclusions

This study comprehensively analyzes the effect of climate on DAC performance and builds on that to provide a regional economic assessment of DAC based on the current best-in-class solid sorbent DAC technology that is commercially available. The most suitable climates and regions for DAC deployment are identified. Colder and drier regions where the temperature does not drop below the DAC operating temperature of −15°C most of the year are the most suitable for DAC when the cost of capital is not taken into account. These regions, however, may not have the cheapest LCOD as regional WACC and cost of energy have a significant impact on LCOD. For instance, at LCOE of \$50 MWh^{-1}, the estimated LCOD for 76% of the world land area, representing regions where temperatures do not drop below −15°C more than 30 days per year, is within the range of \$320–\$540 per tCO_2 due to the effect of regional climates and WACC.

The main limitation of this study is the limited accurate isotherm models for different potential DAC sorbents describing the co-adsorption of CO_2 and H_2O, especially at high RH, and mass transfer models describing the rate of adsorption of CO_2 and H_2O at different ambient temperatures, especially at very low temperatures. This information is needed to assess DAC performance globally and identify suitable sorbents based on regional climates. Future advancements in sorbents, contactor designs or selection of construction materials could provide improved CO_2 productivity with reductions to cost and energy requirements.

Another limitation of this study is that regional variation of LCOE was not addressed, which can affect LCOD. We intend to close this gap in our future work. Future research will assess the regional techno-economic performance of coupling off-grid renewable energy systems with DAC, which can then be compared with coupling DAC to current and future regional electricity grids. This will allow for a more comprehensive regional DAC assessment where regional LCOE and electricity/heat carbon intensity are also considered, which can help identify regions where DAC can be efficiently deployed.

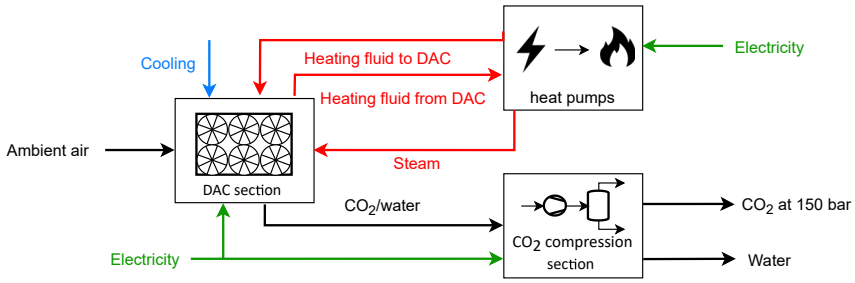

Figure 6. Process flow diagram of the analyzed DAC process

EXPERIMENTAL PROCEDURES

Resource availability

Lead contact

Further information and requests for resources and reagents should be directed to and will be fulfilled by the lead contact, Paul Fennell (p.fennell@imperial.ac.uk).

Materials availability

This study did not generate new unique materials.

Data and code availability

All mathematical models used in this paper are described here in the experimental procedures and in the supplemental information. Global DAC performance data, which are used to generate the global maps in this work, can be obtained from https://doi.org/10.5281/zenodo.7111656.

The DAC process

The DAC process considered in this study is shown in Figure 6. This process consists of two main sections:

- The DAC section, where CO_2 is extracted from the ambient air using CO_2 collectors (i.e., air contactors).
- The CO_2 compression section, where CO_2 is separated from water and compressed to 150 bar.

The CO_2 collector operates a SA-VTSA cycle, mainly consisting of adsorption and desorption cycles, and is modeled based on the solid sorbent-based technology patents.[36,37] During adsorption, fans drive air through the CO_2 collector, where CO_2 and water are adsorbed by the solid sorbent. When the sorbent becomes saturated with CO_2, the collector is sealed and evacuated to vacuum. The desorption step involves heating the sorbent, leading to the desorption of CO_2 and water, which are immediately removed due to the vacuum. Steam purging is then introduced to lower the CO_2 partial pressure inside the collectors and increase the sorbent CO_2 working capacity (i.e., amount of CO_2 that is recovered in each cycle per amount of sorbent). Air source heat pumps provide both process heating and steam. After desorption is completed, the sorbent is cooled down, and then the cycle is repeated.

Adsorption process modeling

The CO_2 collector is modeled based on solid sorbent-based CO_2 collector patents[36,37] using dynamic 1D and 2D adsorption models and a binary CO_2-H_2O isotherm developed for DAC application based on an amine-functionalized sorbent, Lewatit VP OC 1065.[16] Figure 7 shows a visualization of the modeled CO_2 collector. The collectors have a box shape from the outside with dimensions of 1.44, 1.45, and 1.47 m (width, depth, and height). Inside each collector, 88 small thickness (0.01 m) frames are stacked on top of each other in a zigzag fashion to increase the sorbent density per volume of the collector, which helps lower the collector cost. With this arrangement, air can enter on one side of the collector, travel through one of the frames and exit from the opposite side. Each frame is divided using heat transfer tubes into 13 small cells filled with sorbent materials. The heating tubes provide heating and cooling to the sorbents cells from three sides. Moreover, the sorbent cells are enhanced with thin aluminum mesh improving the bed heat transfer.

A rectangular modeling slice that represents a sorbent cell, as shown in Figure 7, is modeled using a combination of dynamic 1D and 2D adsorption models to describe the different cycle steps. Since all sorbent cells are identical inside each collector, the collector performance can be obtained by scaling up the performance of the modeled slice (i.e., multiplying by the number of sorbent cells inside the collector). Combining the 1D and 2D adsorption models can provide better accuracy than using only the 1D model to describe the collector performance without significantly reducing the computational efficiency. While the 2D adsorption model can provide concentration and temperature profiles alongside the sorbent bed (the x-y plane in Figure 7), the 1D model provides faster solution time and the profiles in the flow direction (i.e., z axis), including pressure drop, which is essential in estimating fan energy demand. Therefore, steps where the heating tubes provide heating and cooling are modeled using the 2D model, and other cycle steps are modeled using the 1D model.

The dynamic 1D adsorption model used in this work is similar to the model described in several previous studies.[21,38–41] The model consists of a set of partial differential equations. The main assumptions and features of the 1D adsorption model are as follows:

- Concentration, pressure, and temperature gradients are only considered in the flow direction (z axis).
- The gas phase is described by the ideal gas law.
- Dispersion and conductivity in the flow direction are neglected.
- Thermal equilibrium is established instantaneously between gas and solid phases, including heating elements.
- A linear driving force (LDF) model is used to describe the mass transfer rate.
- The Ergun equation is used to describe the pressure drop.
- Bed voidage and particle diameter are uniform throughout the sorbent bed.
- Heat capacities are independent of temperature.
- Sorbent and the bed (i.e., heat transfer tubes and aluminum mesh) heat capacities are lumped into one term for simplicity.

The overall and component transient mass balance can be mathematically formulated as shown in Equations 1 and 2, respectively,

$$\varepsilon_t \frac{\partial c}{\partial t} + \frac{\partial (uc)}{\partial z} + \rho_b \sum_i^I \frac{\partial q_i}{\partial t} = 0,\ i = CO_2, H_2O, Air, \qquad \text{(Equation 1)}$$

$$\varepsilon_t \frac{\partial c_i}{\partial t} + \frac{\partial (uc_i)}{\partial z} + \rho_b \frac{\partial q_i}{\partial t} = 0,\ i = CO_2, H_2O, Air, \qquad \text{(Equation 2)}$$

where t and z are variables for time and space in the flow direction; c and q are concentration in the gas phase and adsorbed phase, respectively; ε_t and ρ_b are total porosity and bulk density; and u is superficial velocity. In this work, air refers to the dry air mixture that is mostly nitrogen and oxygen, with modeling parameters shown in Note S1.

The energy balance can be expressed mathematically as shown in Equation 3:

$$\left(\varepsilon_t \sum_i^I MW_i c_i Cp_{i,g} + \rho_b Cp_s + \rho_b \sum_i^I MW_i q_i Cp_{i,ads}\right)\frac{\partial T}{\partial t} - \varepsilon_t \frac{\partial P}{\partial t} + u \times \sum_i^I MW_i c_i Cp_{i,g} \frac{\partial T}{\partial z} - \rho_b \sum_i^I \Delta H_{ads,i} \frac{\partial q_i}{\partial t} = 0,\ i = CO_2, H_2O, Air, \qquad \text{(Equation 3)}$$

where MW, Cp, T, P, and ΔH_{ads} are molecular weight, heat capacity, temperature, pressure, and heat of adsorption, respectively; and the subscripts g and ads correspond to the gas phase and adsorption phase, respectively.

The dynamic 2D adsorption model used in this work was developed and experimentally validated by Wurzbacher et al.[14] Similar assumptions to the

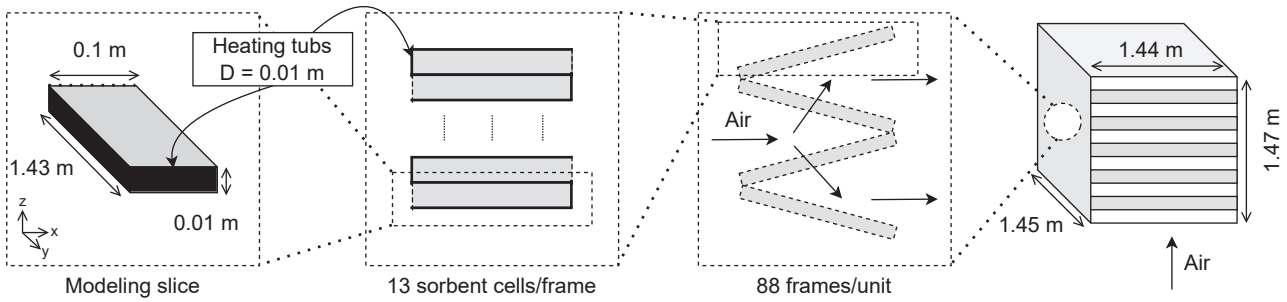

Figure 7. Visualization of the modeled CO_2 collector
The collector is modeled based on solid sorbent-based CO_2 collector patents.[36,37]

1D adsorption model are made for the 2D adsorption model, where the 2D adsorption model key features and assumptions are as follows:

- Concentration and temperature gradients are only considered in the x-y plane.
- The gas phase is described by ideal gas law.
- Constant and uniform pressure throughout the sorbent bed.
- Uniform heating from the wall, and heating tube surface temperature is the same as the fluid temperature.
- Thermal equilibrium is established instantaneously between gas and solid phases.
- Uniform and constant bed thermal conductivity throughout the sorbent bed.
- LDF model is used to describe the mass transfer rate.
- Bed void and particle diameter are uniform throughout the sorbent bed.
- Heat capacities are independent of temperature.
- Sorbent and the bed (i.e., heat transfer tubes and aluminum mesh) heat capacities are lumped in one term for simplicity.

The transient mass balance for the 2D adsorption model is expressed mathematically, as shown in Equations 4 and 5:

$$MW_i\frac{\partial c_i}{\partial t}+\rho_b\,MW_i\frac{\partial q_i}{\partial t}+\nabla\cdot\vec{j_i}+\frac{1}{v_{i,g}}\cdot\left(\rho_b\,MW_{CO_2}\frac{\partial q_{CO_2}}{\partial t}\left(v_{CO_2,ads}-v^P_{CO_2}\right)+\rho_b\,MW_{H_2O}\frac{\partial q_{H_2O}}{\partial t}\left(v_{H_2O,ads}-v^P_{H_2O}\right)+\frac{\partial T}{\partial t}\cdot\frac{\varepsilon_t}{T}-\sum_i^I v_i^P\cdot\nabla\cdot\vec{j_i}\right)=0,\ i=CO_2,H_2O,Air, \quad \text{(Equation 4)}$$

$$\vec{j_i}=-D\cdot\nabla(MW_i\,c_i),\ i=CO_2,H_2O,Air, \quad \text{(Equation 5)}$$

where $\vec{j}$, $v_{i,g}$, v_i^P, ∇, and D are diffusion flux, specific volume of species i at its partial pressure in the gas phase, specific volume of species i at total pressure, del operator, and averaged diffusion coefficient, respectively.

The energy balance mathematical formulation as shown in Equation 6:

$$\left(\varepsilon_t\sum_i^I MW_i\,c_i\,Cp_{i,g}+\rho_b\,Cp_s+\rho_b\sum_i^I MW_i\,q_i\,Cp_{i,ads}\right)\frac{\partial T}{\partial t}=k_{eff}\,\nabla^2T+\rho_b\,\nabla h_{ads,CO_2}\frac{\partial q_{CO_2}}{\partial t}+\rho_b\,\Delta h_{ads,H_2O}\frac{\partial q_{H_2O}}{\partial t}+\varepsilon_t\sum_r MW_i\,Cp_{i,g}\,D(\nabla c_i\cdot\nabla T),\quad i=CO_2,H_2O,Air, \quad \text{(Equation 6)}$$

where k_{eff} is the effective thermal conductivity.

The LDF model is shown in Equation 7:

$$\frac{\partial q_i}{\partial t}=k_i(q_i^*-q_i),\ i=CO_2,H_2O,Air, \quad \text{(Equation 7)}$$

where k is the mass transfer coefficient and q^* is adsorbed phase concentration at equilibrium.

The Ergun equation, which describes the pressure drop across the bed, is shown in Equation 8:

$$\frac{\partial P}{\partial z}=-\frac{150\mu(1-\varepsilon_p)^2}{\varepsilon_p^3d_P^2}u-\frac{1.75\,(1-\varepsilon_p)\rho_g}{\varepsilon_p^3d_P}u^2, \quad \text{(Equation 8)}$$

where μ, ε_p, and d_P are dynamic viscosity, internal porosity, and particle diameter, respectively. The adsorption model parameters are presented in Note S1.

The mechanistic isotherm model developed by Young et al.[16] alongside the single-component Guggenheim-Anderson-de Boer (GAB) isotherm model are used in this work to describe the co-adsorption of CO_2 and H_2O. The equations describing the mechanistic co-adsorption model are shown in Equations 9–16:

$$q^*_{CO_2}=\frac{\varphi}{\varphi_{dry}}\frac{q_\infty(T)b(T)p_{CO_2}}{\left(1+\left(b(T)p_{CO_2}\right)^{\tau(T)}\right)^{\frac{1}{\tau(T)}}}, \quad \text{(Equation 9)}$$

$$q_\infty(T)=q_{\infty,0}e^{\varkappa\left(1-\frac{T}{T_0}\right)}, \quad \text{(Equation 10)}$$

$$b(T)=b_0e^{-\frac{\Delta H_{ave}}{RT}}, \quad \text{(Equation 11)}$$

$$\tau(T)=\tau_0+\alpha\left(1-\frac{T_0}{T}\right), \quad \text{(Equation 12)}$$

$$\varphi=\varphi_{dry}+\left(\varphi_{available}-\varphi_{dry}\right)e^{-\frac{A}{q_{H_2O}}}, \quad \text{(Equation 13)}$$

$$\varphi_{available}=\varphi_{max}-f_{blocked}, \quad \text{(Equation 14)}$$

$$f_{blocked}=f_{blocked,max}\left(1-e^{-\left(kq_{H_2O}\right)^n}\right), \quad \text{(Equation 15)}$$

$$\Delta H_{ave}=\left(1-e^{-\frac{A}{q_{H_2O}}}\right)\Delta H_{dry}+\left(e^{-\frac{A}{q_{H_2O}}}\right)\Delta H_{wet}. \quad \text{(Equation 16)}$$

The equations for the GAB model are shown in Equations 17–22:

$$q^*_{H_2O}=\frac{q_m\,k_{GAB}\,c_{GAB}\,x_{RH}}{(1-k_{GAB}\,x_{RH})(1+(c_{GAB}-1)k_{GAB}\,x_{RH})}, \quad \text{(Equation 17)}$$

$$c_{GAB}=e^{\frac{E_1-E_{10+}}{RT}}, \quad \text{(Equation 18)}$$

$$k_{GAB}=e^{\frac{E_{2-9}-E_{10+}}{RT}}, \quad \text{(Equation 19)}$$

$$E_{10+}=-44.38T+57220, \quad \text{(Equation 20)}$$

$$E_1=C-e^{DT}, \quad \text{(Equation 21)}$$

$$E_{2-9}=F+GT, \quad \text{(Equation 22)}$$

where x_{RH} is RH. The parameters for the isotherm models are presented in Note S2.

The 1D and 2D adsorption models are used to calculate the performance of a modeling cell, shown in Figure 7, which is then scaled up to represent the whole CO_2 collector. The 1D model was discretized along the z axis into equally spaced cells using the finite volume method. To reduce non-physical oscillation in the solution, a van Leer flux limiter[42] was used, and the model was scaled and implemented in dimensionless form, similar to previous work.[43] For the 2D model, since the modeling slice is symmetrical, only one-half of the modeling cell is modeled, then the solution is scaled to represent the whole modeling slice. The 2D model partial differential equations were discretized along the x-y plane into equal-sized cells using finite volumes. The resulting time-dependent ordinary differential equations from the 1D and 2D models were implemented in MATLAB R2021a and solved using ode15s. The boundary conditions along with full description of the SA-VTSA cycle are presented in Notes S3 and S4.

CO_2 compression modeling

The process flow diagram of the CO_2 compression section is shown in Note S5. In this process, the outlet of the DAC section, which mostly contains CO_2 and water, goes through stages of cooling, flash separation, and compression, where the CO_2 is separated from H_2O and compressed to the dense phase of 150 bar. The 150 bar compression pressure is chosen based on previous DAC techno-economic assessment[13] and the assumptions used in the US Department of Energy guidelines[44] for CO_2 transport and sequestration. The maximum outlet temperatures of vacuum pumps and compressors are set to 135°C to maintain their integrity and avoid degradation. Heat at two grades is recovered using heat exchangers. The higher temperature heat is recovered for the sorbent bed heating, whereas the lower temperature heat is recovered to preheat the steam water supply. This section is modeled using Aspen Plus V11 using LKP EOS as it was found to be suitable for a CO_2 and H_2O mixture.[45] More detailed information about the modeling of this process section is found in Note S5.

Process performance indicators

Process productivity for a one DAC collector is calculated as the CO_2 mass recovered ($m_{DAC\ outlet,CO_2}$) per cycle time (t_{cycle}), which can be shown mathematically shown in Equation 23:

$$process\ productivity = \frac{m_{DAC\ outlet,CO_2}}{t_{cycle}}. \quad \text{(Equation 23)}$$

Total heat requirement (Q_{tot}) in MWh per tCO_2 is the sum of the heat consumed for heating the bed (Q_{bed}), heating the steam water supply ($Q_{steam,sens.}$), and generating the steam ($Q_{steam,gen.}$) as shown in Equations 24–27:

$$Q_{tot} = Q_{bed} + Q_{steam,sens.} + Q_{steam,gen.}, \quad \text{(Equation 24)}$$

where

$$Q_{bed} = \frac{1}{m_{DAC\ outlet,CO_2}} \int_0^{t_{des}} \left(\left(\varepsilon_t \sum_i^I MW_i\, c_i\, Cp_{i,g} + \rho_b\, Cp_s + \rho_b \sum_i^I MW_i\, q_i\, Cp_{i,ads} \right) \frac{\partial T}{\partial t} - \rho_b\, \Delta h_{ads,CO_2} \frac{\partial q_{CO_2}}{\partial t} - \rho_b\, \Delta h_{ads,H_2O} \frac{\partial q_{H_2O}}{\partial t} \right) dt\ ,\ i = CO_2, H_2O, Air, \quad \text{(Equation 25)}$$

$$Q_{steam,sens.} = \frac{m_{steam}\ \left(h_{H_2O}(P_{atm}, sat.\ liq) - h_{H_2O}(P_{atm}, T_{amb})\right)}{m_{DAC\ outlet,CO_2}}, \quad \text{(Equation 26)}$$

$$Q_{steam,gen.} = \frac{m_{steam}\ \Delta H_{H_2O,v}\ (P_{atm})}{m_{DAC\ outlet,CO_2}}, \quad \text{(Equation 27)}$$

and m_{steam}, h_{H2O}, P_{atm}, $sat.\ liq$, and $\Delta H_{v,H_2O}$ refer to the mass of steam used, the enthalpy of water, atmospheric pressure, saturated liquid, and water enthalpy of vaporization. When heat is provided by heat pumps, the heat requirement is converted to electrical requirement (E) in MWh per tCO_2 using the COP (Equations 28–31):

$$E_i = \frac{Q_i}{COP}, \quad \text{(Equation 28)}$$

$$COP = \frac{T_H}{T_H - T_C}\eta_{2nd}, \quad \text{(Equation 29)}$$

$$T_H = T_{heating} + \Delta T_{min}, \quad \text{(Equation 30)}$$

$$T_C = T_{ambient} - \Delta T_{min}, \quad \text{(Equation 31)}$$

where η_{2nd}, T_H, T_C, and $T_{heating}$ are second law efficiency, which is assumed to be 50%, heat pump heat sink temperature, heat pump heat source temperature, and heating temperature, respectively. $T_{heating}$ of 110°C is used for steam generation. The total electricity requirements (E_{tot}) when heat pumps are used to provide heat to the process includes electricity consumed to heat the bed ($E_{heating}$), heat the steam water supply ($E_{steam,sens.}$), steam generation ($E_{steam,gen.}$), vacuum pumps and compressors ($E_{comp.}$), and fans (E_{fan}), as shown mathematically in Equation 32:

$$E_{tot} = E_{bed} + E_{steam,sens.} + E_{steam,gen.} + E_{comp.} + E_{fan}, \quad \text{(Equation 32)}$$

where $E_{comp.}$ includes blowdown vacuum pump ($E_{comp.,BL}$) calculated using Equation 33 and other vacuum pumps and compressors in the CO_2 compression and separation section ($E_{comp.,comp.\ sec.}$), which is calculated using Aspen Plus. All vacuum pumps and compressors assume efficiency (η_{comp}) of 70%.

$$E_{comp.,BL} = \frac{\frac{1}{\eta_{comp}} \sum_i^I n_i RT \ln\left(\frac{P_{atm}}{P_{des}}\right)}{m_{DAC\ outlet,CO_2}},\ i = CO_2, H_2O, Air. \quad \text{(Equation 33)}$$

E_{fan} is calculated using the correlation shown in Equation 34:

$$E_{fan} = \frac{\frac{1}{\eta_{fan}} V_{inlet}\ \Delta P_{bed}}{m_{DAC\ outlet,CO_2}}, \quad \text{(Equation 34)}$$

where η_{fan}, V_{inlet}, and ΔP_{bed} are fan efficiency, which is assumed to be 70%, volume of procced air, and pressure drop across the sorbent bed.

Global performance

NASA MERRA-2 hourly temperature and humidity data for 5 years (2016–2020) are used to calculate DAC performance at different locations. The spatial resolution for the dataset is 0.5 × 0.625° (latitude, longitude), which produce a grid with 361 × 576 nodes (n).[46] Using the developed DAC process model, process performance was calculated at 96 data points for an ambient temperature range of 1°C–55°C (12 data points) and RH of 1%–100% (8 data points). The produced dataset can be visualized as 3D gridded data for each of the process performance indicators, with the other two axes corresponding to ambient temperature and RH. This dataset was used to find hourly DAC performance indicators at each node by interpolating the node hourly temperature and RH using MATLAB R2021a spline 3D interpolation. Then, using the produced hourly performance at each node, the node productivity ($productivity_n$) is calculated as the hourly average for all years shown in Equation 35, and the node electricity requirement ($el\ requirement_n$) is calculated as the average electricity requirement for the total produced CO_2 as shown in Equation 36. This approach was used to reduce the computational time required to simulate a whole year using the cyclic adsorption model at each spatial node:

$$productivity_n = \frac{\sum_{h=1}^{hours} hourly\ productivity_{n,h}}{hours}, \quad \text{(Equation 35)}$$

$$el\ requirement_n = \frac{\sum_{h=1}^{hours} hourly\ productivity_{n,h} \times hourly\ el\ requirement_{n,h}}{\sum_{h=1}^{hours} hourly\ productivity_{n,h}}. \quad \text{(Equation 36)}$$

Although sorbents operating at very low ambient temperatures (e.g., −20°C) are being developed,[47,48] it was assumed in this work that the minimum DAC

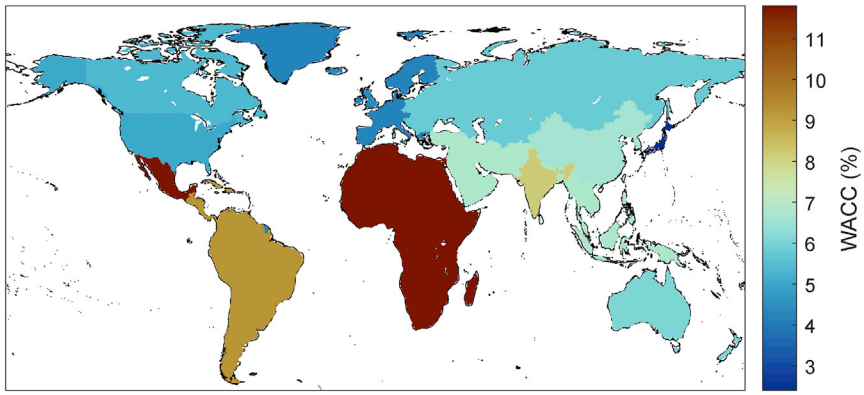

Figure 8. Regional WACC
Adapted from Ameli et al.[30]

process operating temperature is −15°C. This temperature limit is used as a safety design margin as a substantial amount of water is produced and circulated in the process where the chance of water freezing inside pipes and equipment can increase even with good thermal insulation at very low ambient temperatures. This −15°C minimum temperature limit is aligned to what is used in the 1st generation Climeworks unit specification sheet.[49] Moreover, since information about the sorbent (i.e., Lewatit VP OC 1065) performance at low temperatures, including adsorption capacity and mass transfer, is not available, it was assumed that operating at a temperature range of −15°C to –1°C has the same performance as operating at 1°C. A comparison of the model results with an industrial unit is provided Note S6.

Economic analysis

The levelized cost of DAC at each node ($LCOD_n$) is calculated using Equation 37:

$$LCOD_n = \frac{\sum_p (CAPEX_{n,p} \times ACCR_n + OPEX_{n,p}) + OPEX_{sorbent}}{productivity_n} + (LOCE \times el\ requirement_n), \quad \text{(Equation 37)}$$

where *ACCR*, *CAPEX*, and *OPEX* are the annual capital charge ratio, capital expenditures, and operating expenses for process equipment (*p*) calculated using Equations 38–46.[50] *WACC* and *LT* are weighted average capital cost and equipment (or sorbent) lifetime. Lang factor is used to estimate the total cost of the DAC process plant, and relates the purchase cost of major process equipment to the total capital or fixed capital investments, with a Lang factor of 3 assumed in this work.[50] Regional *WACCs* based on low-carbon investments are adopted from Ameli et al.[30] where the world is divided into 16 regions. Figure 8 shows a map of the regional *WACCs*.

$$ACCR = \frac{WACC \times (1+WACC)^{LT}}{(1+WACC)^{LT} - 1} \quad \text{(Equation 38)}$$

$$CAPEX = installed\ Cost + offsite\ Cost + contingency \quad \text{(Equation 39)}$$

$$OPEX = maintenance + overhead \quad \text{(Equation 40)}$$

$$OPEX_{sorbent} = sorbent\ weight \times sorbent\ cost \times ACCR \quad \text{(Equation 41)}$$

$$installed\ Cost = Lang\ Factor \times purchased\ cost \quad \text{(Equation 42)}$$

$$offsite\ Cost = 0.4 \times installed\ Cost \quad \text{(Equation 43)}$$

$$contingency = 0.1 \times (installed\ Cost + offsite\ Cost) \quad \text{(Equation 44)}$$

$$maintenance = 0.03 \times (installed\ Cost + offsite\ Cost) \quad \text{(Equation 45)}$$

$$overhead = 0.65 \times maintenance \quad \text{(Equation 46)}$$

The equipment and sorbent cost assumptions are shown in Table S1. The cost of heat exchangers is neglected as small. The purchased cost for fans and compressors used is based on the maximum equipment size provided in the source. This was done since in this work the size of the DAC plant is not investigated; however, for large-scale DAC deployment, DAC plants will be constructed in a way that takes advantage of economies of scale.

SUPPLEMENTAL INFORMATION

Supplemental information can be found online at https://doi.org/10.1016/j.oneear.2022.09.003.

ACKNOWLEDGMENTS

M.S. is thankful to Saudi Aramco for his PhD scholarship. N.M.D. and P.F. acknowledge funding from UKRI (EPSRC) under grant number EP/P026214/1. We acknowledge the free use of the Scientific Colour Map to prevent visual distortion of the data and exclusion of readers with color-vision deficiencies.[51,52]

AUTHOR CONTRIBUTIONS

Conceptualization, N.M.D. and P.F.; methodology, M.S.; investigation, M.S.; writing – original draft, M.S.; writing – review & editing, M.B., N.M.D., and P.F.; supervision, M.B., N.M.D., and P.F.

DECLARATION OF INTERESTS

The authors declare no competing interests.

Received: May 24, 2022
Revised: June 28, 2022
Accepted: September 26, 2022
Published: October 21, 2022

REFERENCES

1. Royal Society and Royal Academy of Engineering (2018). Greenhouse Gas Removal (Royal Society London).
2. National Academies of Sciences, E., and Medicine (2019). Negative Emissions Technologies and Reliable Sequestration: A Research Agenda (The National Academies Press). https://doi.org/10.17226/25259.
3. Rogelj, J., Popp, A., Calvin, K.V., Luderer, G., Emmerling, J., Gernaat, D., Fujimori, S., Strefler, J., Hasegawa, T., Marangoni, G., et al. (2018). Scenarios towards limiting global mean temperature increase below 1.5 °C. Nat. Clim. Chang. *8*, 325–332. https://doi.org/10.1038/s41558-018-0091-3.
4. Masson-Delmotte, V., Zhai, P., Pörtner, H.-O., Roberts, D., Skea, J., Shukla, P.R., et al. (2018). Global Warming of 1.5 °C (Intergovernmental Panel on Climate Change). https://www.ipcc.ch/sr15/.

5. Fajardy, M., Patrizio, P., Daggash, H.A., and Mac Dowell, N. (2019). Negative emissions: Priorities for research and policy design. Front. Clim. *1*, 6. https://doi.org/10.3389/fclim.2019.00006.

6. Gunnarsson, I., Aradóttir, E.S., Oelkers, E.H., Clark, D.E., Arnarson, M.Þ., Sigfússon, B., Snæbjörnsdóttir, S.Ó., Matter, J.M., Stute, M., Júlíusson, B.M., and Gíslason, S.R. (2018). The rapid and cost-effective capture and subsurface mineral storage of carbon and sulfur at the CarbFix2 site. Int. J. Greenh. Gas Control *79*, 117–126. https://doi.org/10.1016/j.ijggc.2018.08.014.

7. Matter, J.M., Stute, M., Snæbjörnsdottir, S.Ó., Oelkers, E.H., Gislason, S.R., Aradottir, E.S., Sigfusson, B., Gunnarsson, I., Sigurdardottir, H., Gunnlaugsson, E., et al. (2016). Rapid carbon mineralization for permanent disposal of anthropogenic carbon dioxide emissions. Science *352*, 1312–1314. https://doi.org/10.1126/science.aad8132.

8. Scott, V., Haszeldine, R.S., Tett, S.F.B., and Oschlies, A. (2015). Fossil fuels in a trillion tonne world. Nat. Clim. Chang. *5*, 419–423. https://doi.org/10.1038/nclimate2578.

9. Hanna, R., Abdulla, A., Xu, Y., and Victor, D.G. (2021). Emergency deployment of direct air capture as a response to the climate crisis. Nat. Commun. *12*, 368. https://doi.org/10.1038/s41467-020-20437-0.

10. Hepburn, C., Adlen, E., Beddington, J., Carter, E.A., Fuss, S., Mac Dowell, N., Minx, J.C., Smith, P., and Williams, C.K. (2019). The technological and economic prospects for CO_2 utilization and removal. Nature *575*, 87–97. https://doi.org/10.1038/s41586-019-1681-6.

11. McQueen, N., Gomes, K.V., McCormick, C., Blumanthal, K., Pisciotta, M., and Wilcox, J. (2021). A review of direct air capture (DAC): scaling up commercial technologies and innovating for the future. Prog. Energy *3*, 032001. https://doi.org/10.1088/2516-1083/abf1ce.

12. Erans, M., Sanz-Pérez, E.S., Hanak, D.P., Clulow, Z., Reiner, D.M., and Mutch, G.A. (2022). Direct air capture: process technology, techno-economic and socio-political challenges. Energy Environ. Sci. *15*, 1360–1405. https://doi.org/10.1039/D1EE03523A.

13. Keith, D.W., Holmes, G., St. Angelo, D., and Heidel, K. (2018). A process for capturing CO_2 from the atmosphere. Joule *2*, 1573–1594. https://doi.org/10.1016/j.joule.2018.05.006.

14. Wurzbacher, J.A., Gebald, C., Brunner, S., and Steinfeld, A. (2016). Heat and mass transfer of temperature–vacuum swing desorption for CO_2 capture from air. Chem. Eng. J. *283*, 1329–1338. https://doi.org/10.1016/j.cej.2015.08.035.

15. Gebald, C., Wurzbacher, J.A., Tingaut, P., and Steinfeld, A. (2013). Stability of amine-functionalized cellulose during temperature-vacuum-swing cycling for CO_2 capture from air. Environ. Sci. Technol. *47*, 10063–10070. https://doi.org/10.1021/es401731p.

16. Young, J., García-Díez, E., Garcia, S., and van der Spek, M. (2021). The impact of binary water–CO_2 isotherm models on the optimal performance of sorbent-based direct air capture processes. Energy Environ. Sci. *14*, 5377–5394. https://doi.org/10.1039/D1EE01272J.

17. Sabatino, F., Grimm, A., Gallucci, F., van Sint Annaland, M., Kramer, G.J., and Gazzani, M. (2021). A comparative energy and costs assessment and optimization for direct air capture technologies. Joule *5*, 2047–2076. https://doi.org/10.1016/j.joule.2021.05.023.

18. Slesinski, D., and Litzelman, S. (2021). How low-carbon heat requirements for direct air capture of CO_2 can enable the expansion of firm low-carbon electricity generation resources. Front. Clim. *3*. https://doi.org/10.3389/fclim.2021.728719.

19. McQueen, N., Psarras, P., Pilorgé, H., Liguori, S., He, J., Yuan, M., Woodall, C.M., Kian, K., Pierpoint, L., Jurewicz, J., et al. (2020). Cost analysis of direct air capture and sequestration coupled to low-carbon thermal energy in the United States. Environ. Sci. Technol. *54*, 7542–7551. https://doi.org/10.1021/acs.est.0c00476.

20. Madhu, K., Pauliuk, S., Dhathri, S., and Creutzig, F. (2021). Understanding environmental trade-offs and resource demand of direct air capture technologies through comparative life-cycle assessment. Nat. Energy *6*, 1035–1044. https://doi.org/10.1038/s41560-021-00922-6.

21. Stampi-Bombelli, V., van der Spek, M., and Mazzotti, M. (2020). Analysis of direct capture of CO_2 from ambient air via steam-assisted temperature–vacuum swing adsorption. Adsorption *26*, 1183–1197. https://doi.org/10.1007/s10450-020-00249-w.

22. Sinha, A., Darunte, L.A., Jones, C.W., Realff, M.J., and Kawajiri, Y. (2017). Systems design and economic analysis of direct air capture of CO_2 through temperature vacuum swing adsorption using MIL-101(Cr)-PEI-800 and mmen-Mg2(dobpdc) MOF adsorbents. Ind. Eng. Chem. Res. *56*, 750–764. https://doi.org/10.1021/acs.iecr.6b03887.

23. Wijesiri, R.P., Knowles, G.P., Yeasmin, H., Hoadley, A.F.A., and Chaffee, A.L. (2019). Technoeconomic evaluation of a process capturing CO_2 directly from air. Processes *7*, 503. https://doi.org/10.3390/pr7080503.

24. Zhu, X., Ge, T., Yang, F., and Wang, R. (2021). Design of steam-assisted temperature vacuum-swing adsorption processes for efficient CO_2 capture from ambient air. Renew. Sustain. Energy Rev. *137*, 110651. https://doi.org/10.1016/j.rser.2020.110651.

25. Schellevis, H.M., van Schagen, T.N., and Brilman, D.W.F. (2021). Process optimization of a fixed bed reactor system for direct air capture. Int. J. Greenh. Gas Control *110*, 103431. https://doi.org/10.1016/j.ijggc.2021.103431.

26. Breyer, C., Fasihi, M., Bajamundi, C., and Creutzig, F. (2019). Direct air capture of CO_2: a key technology for ambitious climate change mitigation. Joule *3*, 2053–2057. https://doi.org/10.1016/j.joule.2019.08.010.

27. Gebald, C., Repond, N., and Wurzbacher, J.A. (2019). Steam Assisted Vacuum Desorption Process for Carbon Dioxide Capture. patent 10279306B2.

28. Terlouw, T., Treyer, K., Bauer, C., and Mazzotti, M. (2021). Life cycle assessment of direct air carbon capture and storage with low-carbon energy sources. Environ. Sci. Technol. *55*, 11397–11411. https://doi.org/10.1021/acs.est.1c03263.

29. Fuss, S., Lamb, W.F., Callaghan, M.W., Hilaire, J., Creutzig, F., Amann, T., et al. (2018). Negative emissions—Part 2: costs, potentials and side effects. Environ. Res. Lett. *13*, 063002. https://doi.org/10.1088/1748-9326/aabf9f.

30. Ameli, N., Dessens, O., Winning, M., Cronin, J., Chenet, H., Drummond, P., Calzadilla, A., Anandarajah, G., and Grubb, M. (2021). Higher cost of finance exacerbates a climate investment trap in developing economies. Nat. Commun. *12*, 4046. https://doi.org/10.1038/s41467-021-24305-3.

31. Viebahn, P., Scholz, A., and Zelt, O. (2019). The potential role of direct air capture in the German energy research Program—results of a multi-dimensional analysis. Energies *12*, 3443. https://doi.org/10.3390/en12183443.

32. Cheng, V.K., and Hammond, G.P. (2017). Life-cycle energy densities and land-take requirements of various power generators: a UK perspective. J. Energy Inst. *90*, 201–213. https://doi.org/10.1016/j.joei.2016.02.003.

33. Ong, S., Campbell, C., Denholm, P., Margolis, R., and Heath, G. (2013). Land-use Requirements for Solar Power Plants in the United States (National Renewable Energy Laboratory).

34. Bui, M., Adjiman, C.S., Bardow, A., Anthony, E.J., Boston, A., Brown, S., Fennell, P.S., Fuss, S., Galindo, A., Hackett, L.A., et al. (2018). Carbon capture and storage (CCS): the way forward. Energy Environ. Sci. *11*, 1062–1176. https://doi.org/10.1039/C7EE02342A.

35. Deutz, S., and Bardow, A. (2021). Life-cycle assessment of an industrial direct air capture process based on temperature–vacuum swing adsorption. Nat. Energy *6*, 203–213. https://doi.org/10.1038/s41560-020-00771-9.

36. Gebald, C., Piatkowski, N., Rüesch, T., and Wurzbacher, J.A. (2014). Low-pressure drop structure of particle adsorbent bed for adsorption gas separation process. WIPO patent WO2014170184A1, filed April 9, 2014, and published October 23, 2014.

37. Gebald, C., Meier, W., Repond, N., Rüesch, T., and Wurzbacher, J.A. (2017). Direct air capture device. US patent US20170106330A1, filed May 28, 2015, and published April 20, 2017.

38. Haghpanah, R., Majumder, A., Nilam, R., Rajendran, A., Farooq, S., Karimi, I.A., and Amanullah, M. (2013). Multiobjective optimization of a four-step adsorption process for postcombustion CO_2 Capture via Finite Volume Simulation. Ind. Eng. Chem. Res. *52*, 4249–4265. https://doi.org/10.1021/ie302658y.

39. Casas, N., Schell, J., Pini, R., and Mazzotti, M. (2012). Fixed bed adsorption of CO_2/H_2 mixtures on activated carbon: experiments and modeling. Adsorption *18*, 143–161. https://doi.org/10.1007/s10450-012-9389-z.

40. Javeed, S., Qamar, S., Seidel-Morgenstern, A., and Warnecke, G. (2011). Efficient and accurate numerical simulation of nonlinear chromatographic processes. Comput. Chem. Eng. *35*, 2294–2305. https://doi.org/10.1016/j.compchemeng.2010.10.002.

41. Webley, P.A., and He, J. (2000). Fast solution-adaptive finite volume method for PSA/VSA cycle simulation; 1 single step simulation. Comput. Chem. Eng. *23*, 1701–1712. https://doi.org/10.1016/S0098-1354(99)00320-8.

42. LeVeque, R.J. (2002). Finite Volume Methods for Hyperbolic Problems (Cambridge University Press).

43. Hasan, M.M.F., Baliban, R.C., Elia, J.A., and Floudas, C.A. (2012). Modeling, simulation, and optimization of postcombustion CO_2 capture for variable feed concentration and flow rate. 2. Pressure swing adsorption and vacuum swing adsorption processes. Ind. Eng. Chem. Res. *51*, 15665–15682. https://doi.org/10.1021/ie301572n.

44. Shirley, P., and Myles, P. (2019). Quality Guidelines for Energy System Studies: CO_2 Impurity Design Parameters (National Energy Technology Laboratory).

45. White, C.W., and Weiland, N.T. (2018). Evaluation of Property methods for modeling direct-supercritical CO_2 power cycles. J. Eng. Gas Turbine. Power *140*, 011701. https://doi.org/10.1115/1.4037665.

46. Gelaro, R., McCarty, W., Suárez, M.J., Todling, R., Molod, A., Takacs, L., Randles, C., Darmenov, A., Bosilovich, M.G., Reichle, R., et al. (2017). The modern-era retrospective analysis for research and applications, version 2 (MERRA-2). J. Clim. *30*, 5419–5454. https://doi.org/10.1175/jcli-d-16-0758.1.

47. Rim, G., Kong, F., Song, M., Rosu, C., Priyadarshini, P., Lively, R.P., and Jones, C.W. (2022). Sub-ambient temperature direct air capture of CO_2 using amine-impregnated MIL-101(Cr) enables ambient temperature CO_2 recovery. JACS Au *2*, 380–393. https://doi.org/10.1021/jacsau.1c00414.

48. Song, M., Rim, G., Kong, F., Priyadarshini, P., Rosu, C., Lively, R.P., and Jones, C.W. (2022). Cold-temperature capture of carbon dioxide with water coproduction from air using commercial zeolites. Ind. Eng. Chem. Res. *61*, 13624–13634. https://doi.org/10.1021/acs.iecr.2c02041.

49. Climeworks. DAC1 data sheet – Capturing CO_2 from air. https://www.venturelab.swiss/demandit/files/M_BB941CC4DCEF687AD98/dms/File/CLIMEWORKS_productsheet_P_mail.pdf. [Accessed October 10, 2022].

50. Towler, G., and Sinnott, R. (2021). Chemical Engineering Design: Principles, Practice and Economics of Plant and Process Design (Butterworth-Heinemann).

51. Crameri, F. (2018). Scientific colour-maps. Zenodo *10*. https://doi.org/10.5281/zenodo.1243862.

52. Crameri, F., Shephard, G.E., and Heron, P.J. (2020). The misuse of colour in science communication. Nat. Commun. *11*, 5444. https://doi.org/10.1038/s41467-020-19160-7.